

# More on the structure of tidal tails

Andreas H.W. Küpper<sup>1,2\*</sup>, Richard R. Lane<sup>3</sup> and Douglas C. Heggie<sup>4</sup>

<sup>1</sup>*Argelander Institut für Astronomie (AIfA), Auf dem Hügel 71, 53121 Bonn, Germany*

<sup>2</sup>*European Southern Observatory, Alonso de Cordova 3107, Vitacura, Santiago, Chile*

<sup>3</sup>*Departamento de Astronomía, Universidad de Concepción, Casilla 160 C, Concepción, Chile*

<sup>4</sup>*University of Edinburgh, School of Mathematics and Maxwell Institute for Mathematical Sciences, King's Buildings, Edinburgh EH9 3JZ*

Accepted .... Received ...; in original form ...

## ABSTRACT

We investigate the epicyclic motion of stars escaping from star clusters. Using streaklines, we visualise the path of escaping stars and show how epicyclic motion leads to over- and underdensities in tidal tails of star clusters moving on circular and eccentric orbits about a galaxy. Additionally, we investigate the effect of the cluster mass on the tidal tails, by showing that their structure is better matched when the perturbing effect of the cluster mass is included. By adjusting streaklines to results of  $N$ -body computations we can accurately and quickly reproduce all observed substructure, especially the streaky features often found in simulations which may be interpreted in observations as multiple tidal tails. Hence, we can rule out tidal shocks as the origin of such substructures. Finally, from the adjusted streakline parameters we can verify that for the star clusters we studied escape mainly happens from the tidal radius of the cluster, given by  $x_L = (GM/(\Omega^2 - \partial^2\Phi/\partial R^2))^{1/3}$ . We find, however, that there is another limiting radius, the “edge” radius, which gives the smallest radius from which a star can escape during one cluster orbit about the galaxy. For eccentric cluster orbits the edge radius shrinks with increasing orbital eccentricity (for fixed apocentric distance) but is always significantly larger than the respective perigalactic tidal radius. In fact, the edge radii of the clusters we investigated, which are extended and tidally filling, agree well with their (fitted) King radii, which may indicate a fundamental connection between these two quantities.

**Key words:** methods: numerical – globular clusters – Galaxy: kinematics and dynamics – galaxies: star clusters: general

## 1 INTRODUCTION

Tidal tails of galactic satellites like dwarf spheroidal galaxies and globular clusters are interesting structures as they tell the story of the dynamical past of the corresponding object. The most prominent feature of tidal tails is their large extent across their host galaxy (Yanny et al. 2003; Grillmair & Johnson 2006; Grillmair & Dionatos 2006a,b). From the shape of extended tidal tails it is possible to infer the orbit of their progenitor satellite (Lin & Lynden-Bell 1977; Lynden-Bell & Lynden-Bell 1995; Peñarrubia et al. 2005; Belokurov et al. 2006; Fellhauer et al. 2006). The constraints on the satellite orbit can be further improved when radial velocity or proper motion data of tidal tail stars is available (Johnston et al. 1999; Law, Johnston & Majewski 2005;

Binney 2008; Eyre & Binney 2009a,b; Odenkirchen et al. 2009; Koposov, Rix & Hogg 2010).

Tidal tails, however, also contain additional information. Variations of the stellar density along the tails have been observed for extended tidal streams such as the Milky Way globular cluster Palomar 5 (Odenkirchen et al. 2003). For other Milky Way satellites, such as NGC 288, Willman 1 and NGC 2298, multiple tidal tails have been observed (Leon, Meylan & Combes 2000; Willman et al. 2006; Balbinot et al. 2011). This substructure should also be somehow linked to the dynamical past of the satellite.

In the common picture, substructure is created by tidal variations, such as tidal shocks, which temporarily increase the mass loss rate of the satellite (Gnedin & Ostriker 1997). Tidal tails which are produced in such a violent way should be dynamically hotter and thus broader than tails originating from dynamical evaporation. Extended satellites like dwarf spheroidal galaxies often show such tidal streams (e.g. Grillmair 2006) but tidal tails of star clusters appear to be typically more compact and colder (Grillmair & Johnson

\* E-mail: akuepper@astro.uni-bonn.de (AHWK);  
rlane@astro-udec.cl (RRL); dcheggie@ed.ac.uk (DCH)

2006; Grillmair & Dionatos 2006b) suggesting that they are mainly being produced by dynamical evaporation.

In numerical investigations it has been shown that for star clusters, tidal variations have to be, in fact, very extreme in order to cause substructure in their tidal tails (Dehnen et al. 2004; Küpper et al. 2010a). This is due to the compactness of star clusters which makes them less vulnerable to tidal stripping. Observed substructure in tidal tails of star clusters is, therefore, most likely not due to tidal variations.

On the contrary, it has been shown that substructure can even arise in tidal tails of star clusters which move in a steady tidal field (Capuzzo Dolcetta, Di Matteo & Miocchi 2005; Küpper, MacLeod & Heggie 2008a; Just et al. 2009; Küpper et al. 2010a). This substructure is caused by the epicyclic motion performed by a continuous stream of stars evaporating from the cluster. It has been shown analytically and numerically that this substructure can be related to the internal properties of the star cluster (its mass) and its external properties (its orbit about the galaxy). Moreover, star clusters on eccentric orbits were also found to produce tidal tail substructure in this way, rather than through tidal shocks (Küpper et al. 2010a).

However, clumps in tidal tails may also be produced when parts of a stellar stream pass a spiral arm, a giant molecular cloud or a massive dark-matter subhalo (e.g. Ibata et al. 2002; Carlberg 2009). Therefore, the understanding of the formation of substructure in tidal tails is of vital importance when interpreting observations of clumpy tidal tails.

In the present investigation we show with the help of streaklines exactly how the epicyclic motion of escaping stars leads to substructure in tidal tails of star clusters on circular and eccentric orbits (Sec. 2). Then we compare results from  $N$ -body computations to theoretical streaklines to visualise the path of escaping stars and to demonstrate the accuracy of the much more rapid method of streaklines (Sec. 3). In the last Section we give a brief summary and discuss our results.

## 2 THEORY

Due to energy equipartition, stars in a star cluster permanently exchange energy. This process is called two-body relaxation and leads to the continuous escape of stars from the cluster, since again and again some stars gain energies above the escape energy (see e.g. Heggie & Hut 2003). However, in most cases, even if they are energetically unbound, stars will stay within the cluster for several dynamical timescales. These “potential escapers”, are preferentially located at large cluster radii where the dynamical timescale is of the order of the orbital timescale of the star cluster about the Galaxy (Gnedin, Lee & Ostriker 1999; Fukushige & Heggie 2000; Küpper et al. 2010b). In fact, a flattening of the velocity dispersion profile has been observed in the outer parts of Milky Way globular clusters like 47 Tucanae (Drukier et al. 1998; Scarpa et al. 2007; Lane et al. 2009; Scarpa & Falomo 2010; Lane et al. 2010a,b; Scarpa et al. 2011), which may well be interpreted as the contribution from potential escapers.

External energy which is added to a cluster, for in-

stance through tidal shocks, is redistributed within the cluster in the same way. The additional energy causes more stars to escape from the cluster in a given time interval but does not immediately influence the structure of the cluster (Baumgardt & Makino 2003; Küpper et al. 2010b). For this reason tidal shocks do not inevitably lead to substructure in tidal tails as the escape of unbound stars is delayed with respect to the tidal shock (Küpper et al. 2010a). Note that this may be significantly different for extended objects with large relaxation times such as dwarf spheroidal galaxies, especially when they are on very eccentric orbits about their host galaxy (c.f. Peñarrubia et al. 2009).

Inside the cluster, each star moves within the gravitational field of the other cluster stars plus the external tidal field of the galaxy. In the cluster reference frame, in which the cluster is at rest, the motion of stars is complicated by the Coriolis, centrifugal and Euler pseudo forces resulting from the cluster’s orbital motion about the galactic centre (see e.g. Chandrasekhar 1942). This effective potential of the cluster is attractive towards the cluster centre within the tidal sphere with radius  $x_L$ . This radius gives the distance to the Lagrange points from the cluster centre along the radial direction connecting the galactic centre with the cluster centre, i.e. the radius at which the cluster attraction equals the effective force of the external field. It is often denoted as the tidal radius and can be approximated for circular cluster orbits in a Milky Way-like potential as

$$x_L \simeq \left( \frac{GM}{2\Omega^2} \right)^{1/3}, \quad (1)$$

where  $G$  is the gravitational constant,  $M$  is the cluster mass, and  $\Omega$  is the cluster’s angular velocity about the galactic centre (see e.g. King 1962; Just et al. 2009; Küpper et al. 2010a). For eccentric cluster orbits the tidal radius can be calculated using

$$x_L = \left( \frac{GM}{\Omega^2 - \partial^2 \Phi / \partial R^2} \right)^{1/3}, \quad (2)$$

where  $\Phi$  is the galactic potential and  $R$  is the cluster’s galactocentric distance (e.g. Küpper et al. 2010a). Due to the dependence on  $\Omega$ , the tidal radius can change significantly between peri- and apogalacticon for clusters on eccentric orbits. When a star evaporates from a cluster it will most likely escape through one of the two Lagrange points  $L_1$  (closer to the galactic centre) or  $L_2$  (further away from the galactic centre), since escape is easiest through these points, finally ending up in the leading or trailing tidal tail, respectively.

Note that the estimate of the limiting radius (Eq. 2) was derived for a star instantaneously situated between the cluster and the galactic centre (see King 1962). Considerable subsequent research has shown that stars well outside this estimate of the limiting radius may well remain attached to the cluster, for example those on appropriate retrograde orbits (Read et al. 2006). Hence, we should keep in mind that at any time there will be stars outside the radius  $x_L$  which are actually still bound to the cluster, and that there are stars escaping from radii smaller than  $x_L$ .

Outside the tidal radius, the effective potential is repulsive in some directions such that stars feel a drag away from the cluster once they escape from its tidal sphere. Hence, the gravitational field of the cluster quickly becomes unimportant for the motion of the escapers. Within the tails the

stars will perform an epicyclic motion due to the pseudo forces mentioned above (plus the tidal force), in which the stars will be periodically accelerated and decelerated while moving along the tidal tails. How this epicyclic motion looks depends on the escape conditions of the stars. In the case where the escape conditions of many escaping stars are similar, their epicyclic motions will lead to an over- and under-density pattern. This is a statistical effect, which is due to the fact that there is a higher probability for the presence of stars within the epicyclic cusps than in between two cusps.

In the following we briefly review how the epicyclic motions of escaping stars depend on the escape conditions. For three different star cluster models we then show how the orbit influences the epicyclic trajectories of escaping stars. Moreover, we demonstrate the influence of the cluster mass on these trajectories. Since the stellar trajectories cannot be calculated analytically for clusters on eccentric orbits or when the cluster mass is taken into account, we use streaklines as often applied in fluid dynamics to visualise the tracks of escaping stars (see Sec. 2.3).

## 2.1 Epicyclic motion

In Küpper, MacLeod & Heggie (2008a) it was shown for star clusters on circular orbits that, in a coordinate system in which the cluster is at rest (x-axis points towards the galactic anticentre, y-axis points into the direction of cluster motion), the length of an escaper's epicycle along the corresponding tidal tail (leading or trailing),  $y_C$ , can be analytically related to the tidal radius,  $x_L$ , of the cluster by

$$y_C = \frac{4\pi\Omega}{\kappa} \left( 1 - \frac{4\Omega^2}{\kappa^2} \right) x_L, \quad (3)$$

where  $\kappa$  is the epicyclic frequency of the specific galactic potential. For clusters in Milky Way-like tidal fields  $\kappa \simeq 1.4\Omega$  holds (Just et al. 2009), such that Eq. 3 reduces to

$$y_C \simeq 3\pi x_L. \quad (4)$$

In this calculation it is assumed that the escaping star evaporates from one of the two Lagrange points and has exactly the same angular velocity,  $\Omega$ , as the cluster at the moment of escape. Moreover, the influence of the gravitational attraction of the cluster is neglected in this ansatz.

Just et al. (2009) found a more general solution for the length of the epicycles,

$$y_C = \frac{4\pi}{\beta} \frac{\beta^2 - 4}{\beta^2} \left( \Delta x + \frac{v_t}{2\Omega} \right), \quad (5)$$

where  $\beta = \kappa/\Omega$ ,  $\Delta x$  is some distance from the cluster centre to the point of escape along the radial direction connecting cluster centre and galactic centre, and  $v_t$  is some additional velocity along the cluster orbit in the direction of the corresponding tail. For a Milky Way-like potential this simplifies to

$$y_C \simeq 3\pi \left( \Delta x + \frac{v_t}{2\Omega} \right), \quad (6)$$

which gives Eq. 4 for  $\Delta x = x_L$  and  $v_t = 0$ . Therefore, if a star escapes from a radius larger or smaller than the tidal radius, the epicycle gets larger or smaller, respectively. Furthermore, an additional tangential velocity in the direction of the corresponding tail will increase the epicycle length of

a star, whereas an additional tangential velocity in the opposite direction to the corresponding tail will decrease the epicycle length.

The radial offset and the radial amplitude of the epicyclic motion (the x-component of the epicyclic motion) was derived analytically by Just et al. (2009). This part of the epicyclic movement depends on the initial radial offset,  $\Delta x$ , and on the additional tangential velocity along the tidal tails,  $v_t$ . It is given by

$$x_m = \frac{1}{\beta^2} \left( 4\Delta x + \frac{v_t}{\Omega} \pm \left| (4 - \beta^2) \Delta x + \frac{2v_t}{\Omega} \right| \right), \quad (7)$$

where we corrected a typo in the original Just et al. equation. This amplitude reduces in a Milky Way-like potential to

$$x_m \simeq 2\Delta x + \frac{v_t}{\Omega} \pm \left| \Delta x + \frac{v_t}{\Omega} \right|, \quad (8)$$

that is if  $v_t$  is zero then the escapers oscillate around a radius of  $2\Delta x$  with an amplitude of  $2\Delta x$ .

In Küpper et al. (2010a) it was shown with a comprehensive set of  $N$ -body models that the epicycles of escaping stars from clusters on circular orbits are on average a bit larger than predicted when assuming  $\Delta x = x_L$  and  $v_t = 0$ . In the framework of this theory, this increase in length can be due to both  $\Delta x > x_L$  or  $v_t > 0$ . In the following we will demonstrate that this discrepancy is, in fact, due to the neglected cluster mass. Since there is no simple analytical solution to the problem when the cluster mass is taken into account, we can only prove this assumption numerically, which will be done using streaklines.

Furthermore, it was demonstrated in Küpper et al. (2010a) that epicyclic motion of escaping stars also leads to over- and underdensities in tidal tails of star clusters moving on eccentric orbits. Even though the shape and density distribution along the tails gets significantly more complicated for such clusters, it was shown that the distance of the epicyclic overdensities could be related to a mean escape radius and a mean escape velocity. Due to the periodic acceleration and deceleration of the cluster and the tail stars within the orbit about the galactic centre, the distance from the cluster to the overdensities periodically increases or decreases, respectively. For this problem there is no simple analytical solution either, therefore, in the following we are also going to visualise the trajectories of escaping stars for such cluster orbits using streaklines.

## 2.2 Models

We investigate the epicyclic motion of tail stars for three different types of cluster orbits. First of all, we look at the circular orbit case, then we look at two eccentric orbits with eccentricities,  $\epsilon$ , of 0.25 and 0.5. The eccentricity is defined as

$$\epsilon = \frac{R_{apo} - R_{peri}}{R_{apo} + R_{peri}}, \quad (9)$$

where  $R_{apo}$  is the cluster's apogalactic distance and  $R_{peri}$  its perigalactic distance. A circular orbit therefore has an eccentricity of 0.

For the integration of the orbits we use the Milky Way-like potential suggested by Allen & Santillan (1991). This galactic potential,  $\Phi$ , consists of a central point-mass potential given by

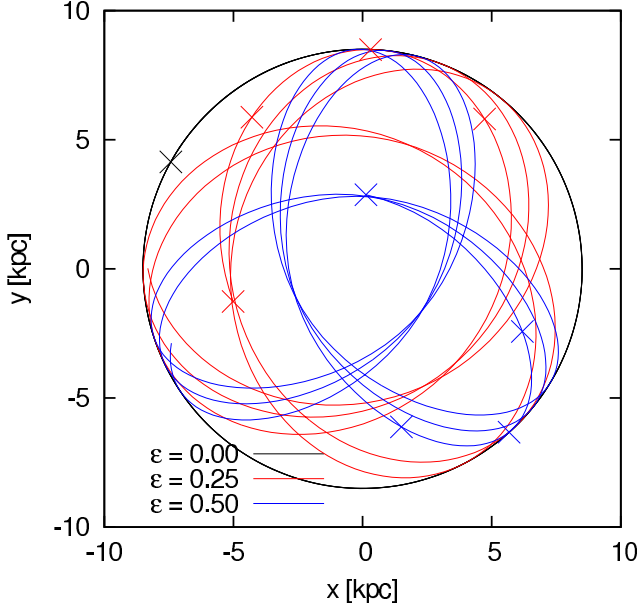


**Figure 1.** Orbits of the three  $N$ -body models which were used in this analysis for comparison with the theoretical streaklines. One model is on a circular orbit, one has an orbital eccentricity of 0.25 and the third model follows an orbit with an eccentricity of 0.5. The crosses mark the orbital phases where snapshots were taken for analysis (see also Tab. 1).

**Table 1.** Overview of the snapshots from the three cluster models which are investigated in detail. The columns give the orbital eccentricity,  $\epsilon$  (Eq. 9), the apogalactic distance,  $R_{apo}$ , the perigalactic distance,  $R_{peri}$ , and the galactocentric distance,  $R_{GC}$ , of the cluster. The orbital phase,  $p_{orb}$ , is defined by Eq. 14. The two last columns give the orbital velocity,  $v_{orb}$ , and the angular velocity,  $\Omega$ , of the cluster at the time of the snapshot.

$\epsilon$	$R_{apo}$ [kpc]	$R_{peri}$ [kpc]	$R_{GC}$ [kpc]	$p_{orb}$	$v_{orb}$ [kms $^{-1}$ ]	$\Omega$ [Myr $^{-1}$ ]
0.00	8.5	8.5	8.5	1.00	220	0.026
0.25	8.5	5.1	8.5	1.00	165	0.019
			7.3	-0.65	205	0.028
			5.2	-0.03	272	0.052
			7.5	0.71	198	0.026
0.50	8.5	2.8	8.5	1.00	110	0.013
			6.6	-0.67	189	0.029
			2.9	0.02	330	0.114
			6.3	0.61	201	0.032

$$\Phi_c(R) = -\frac{M_1}{\sqrt{R^2 + b_1^2}}, \quad (10)$$

a Miyamoto & Nagai (1975) disk potential given by

$$\Phi_d(x, y, z) = -\frac{M_2}{\sqrt{x^2 + y^2 + \left(a_2 + \sqrt{z^2 + b_2^2}\right)^2}}, \quad (11)$$

and a halo potential of the form

$$\Phi_h(R) = -\frac{M(R)}{R} - \frac{M_3}{1.02a_3} \quad (12)$$

$$\left[ -\frac{1.02}{1 + (R/a_3)^{1.02}} + \ln \left( 1 + (R/a_3)^{1.02} \right) \right]_R^{100},$$

where

$$M(R) = \frac{M_3(R/a_3)^{2.02}}{1 + (R/a_3)^{1.02}}. \quad (13)$$

The numerical constants  $M_1$ ,  $b_1$ ,  $M_2$ ,  $a_2$ ,  $b_2$ ,  $M_3$  and  $a_3$  are chosen such that the combined potential of the three components has a circular velocity of 220 kms $^{-1}$  at 8.5 kpc (see Allen & Santillan 1991).

The apogalactic distance of all three clusters is 8.5 kpc (which is a somewhat arbitrary choice). Therefore, the circular orbit has a constant orbital velocity,  $v_{orb}$ , of 220 kms $^{-1}$ , whereas the eccentric orbits have an orbital velocity of 165 kms $^{-1}$  and 110 kms $^{-1}$  at apogalacticon for an eccentricity of 0.25 and 0.5, respectively. Their perigalactic distances are 5.1 kpc and 2.8 kpc, respectively, and their velocities at these orbital phases are 275 kms $^{-1}$  and 334 kms $^{-1}$ . The orbital timescale is 240 Myr for the circular case, 133 Myr for  $\epsilon = 0.25$  and 113 Myr for  $\epsilon = 0.5$ . An overview of these quantities is given in Tab. 1. In Fig. 1 the integrated orbits are shown for 400 Myr.

The shape and structure of tidal tails for star clusters on eccentric orbits is strongly influenced by the orbital phase of the cluster (Küpper et al. 2010a; Küpper, Mieske & Kroupa 2011a). To illustrate the changes between the different orbital phases, we pick four snapshots from the integrations of each of the two eccentric orbits. The snapshots are taken in steps of 30 Myr starting from apogalacticon. In the next snapshots the clusters are in an orbital phase between apogalacticon and perigalacticon in which the clusters are accelerated towards the galactic centre. The third snapshots are close to perigalacticon, and the last ones are between perigalacticon and apogalacticon in which the clusters and their tails are decelerated. The points at which those snapshots were taken are illustrated in Fig. 1 as crosses.

One way to quantify the orbital phase,  $p_{orb}$ , of a star cluster in its orbit about the galaxy is given in Küpper, Mieske & Kroupa (2011a) by

$$p_{orb} = \frac{\dot{R}_{GC}}{|\dot{R}_{GC}|} \frac{R_{GC} - R_{peri}}{R_{apo} - R_{peri}}, \quad (14)$$

where  $R_{GC}$  is the cluster's current galactocentric radius, and  $\dot{R}_{GC}$  is the time derivative of this radius. In this way, the orbital phase is zero at perigalacticon and unity at apogalacticon (in fact  $\pm 1$ ). Moreover, it is negative when the cluster is moving to perigalacticon and positive if its moving to apogalacticon. The orbital phases of the cluster snapshots which we investigate in detail are given in Tab. 1.

### 2.3 Streaklines

In Küpper, MacLeod & Heggie (2008a) and Just et al. (2009) it was shown that the orbits of stars escaping from a cluster can, under certain assumptions, be integrated analytically. In this simplified case a star is released from the cluster centre with a certain positive or negative offset along the galactocentric radius, and with some negative or positive offset velocity with respect to the cluster. One of the main assumptions here is that the cluster moves in a circular or-

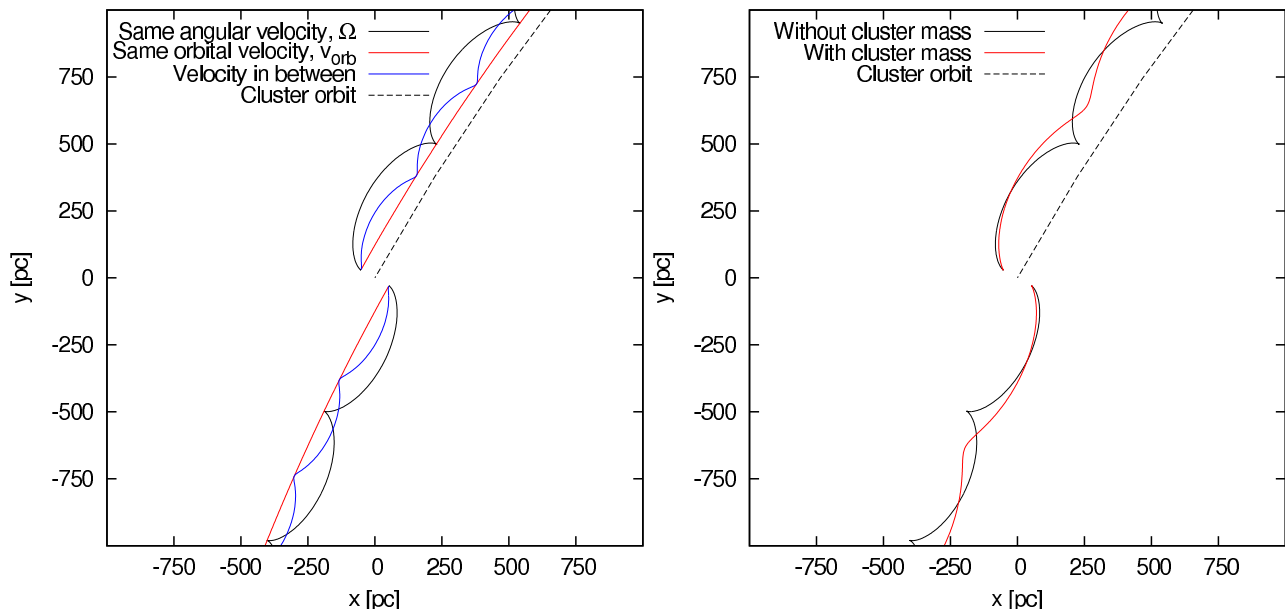


**Figure 2.** Snapshot of the cluster model on a circular orbit (black dashed lines). Left panel: to produce the three sets of streaklines, test particles were released during the last few hundred Myr of this numerical integration from two radial offsets,  $\pm\Delta x$  (which we chose to be 60 pc in this example), with respect to the cluster orbit, and with three different tangential velocities,  $v_t$ . The black solid lines show the streaklines resulting from the test particles being released with the same angular velocity as the cluster. The epicyclic motion as described in Küpper, MacLeod & Heggie (2008a) is nicely reproduced. The red solid lines show the path of the test particles which have the same orbital velocity as the cluster. Just like the cluster they move on circular orbits about the galactic centre. The blue solid lines show the test particles with velocities in between these two cases. The length of the epicycles is shorter and the radial amplitude is smaller. The cluster mass was neglected in these calculations. Right panel: here the effect of the cluster mass on the trajectories of the test particles is shown. The cluster mass was chosen such that the tidal radius is 60 pc. The black solid lines are the same as in the left panel, whereas the red solid lines show the influence of the cluster mass: the sharp cusp is replaced by a smooth minimum, which, in addition, is further away from the cluster. Moreover, the test particles are, on average, further away from the cluster orbit in radial direction.

bit about the galactic centre. Moreover, the cluster mass is neglected in this calculation.

For eccentric cluster orbits such a general analytical solution does not exist. In addition, the trajectories of escaping stars depend on the orbital phase of the cluster in this case. Instead of solving the equations of motion analytically, we can simply illustrate the trajectories of stars for eccentric cluster orbits by using streaklines. This is a concept from fluid dynamics in which test particles are released into a fluid from a given point to visualise the flow. In engineering streaklines are often produced with smoke or dye.

To produce the streaklines we integrate the cluster orbit and, at given time intervals, release test particles. These particles have a certain velocity,  $v$ , and are released from two points which are given by the cluster centre plus a fixed positive or negative radial offset,  $\Delta x$ , along the galactocentric radius vector. All released test particles are then integrated together with the cluster to the point in time of the snapshot. The gravitational influence of the cluster on the test particles is taken into account in the cases where it is mentioned explicitly. There is no interaction between the test particles.

For this purpose, it is not reasonable to stay within the rotating, accelerated reference frame in which a cluster on a circular orbit is at rest, for which the analytical solutions of Küpper, MacLeod & Heggie (2008a) and Just et al. (2009) have been developed. Thus, we have to keep in mind that we have to convert the tangential offset velocities in the rotating

coordinate system,  $v_t$ , to the Cartesian, galactocentric rest frame velocities,  $v$ , when applying Eq. 6.

First we illustrate that the technique works correctly by comparing it with results from the formalism described in Sec. 2.1 for circular orbits. Therefore, we produce three sets of streaklines in which the test particles are released with three different velocities,  $v$ , from the cluster on a circular orbit:

- (i) the test particles are released with the same angular velocity as the cluster,  $\Omega$ , i.e. the test particles which are released from the larger galactocentric radius have a higher orbital velocity than the cluster,  $v = v_{orb} + \Omega\Delta x$ , whereas the test particles at the smaller galactocentric radius have a lower orbital velocity,  $v = v_{orb} - \Omega\Delta x$ . This corresponds to the case  $v_t = 0$  in Eq. 6,
- (ii) the test particles have the same orbital velocity as the cluster, i.e.  $v = v_{orb}$ . This corresponds to  $v_t = -\Omega\Delta x$  in Eq. 6,
- (iii) the test particles have an orbital velocity in between the two cases, i.e.  $v_t = -0.5\Omega\Delta x$  corresponding in the galactocentric rest frame to  $v = v_{orb} + 0.5\Omega\Delta x$  for the leading tail and  $v = v_{orb} - 0.5\Omega\Delta x$  for the trailing tail, respectively.

These sets of streaklines we also produce for the eccentric orbits to see how the orbital acceleration and deceleration influence the trajectories of escaping stars.

Finally, we produce additional sets of streaklines for which the mass of the cluster is taken into account. The

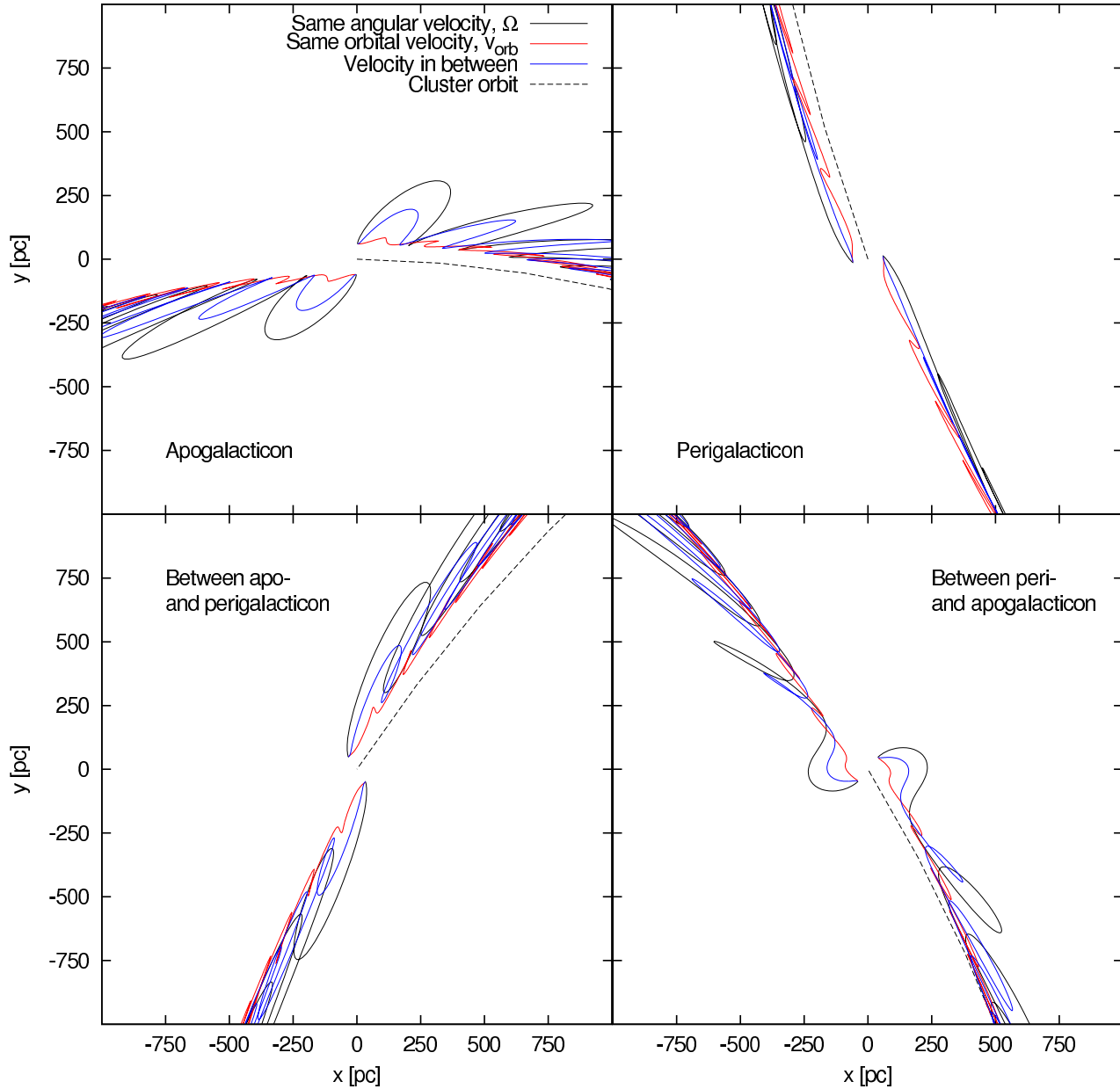


**Figure 3.** The same as in the left panel of Fig. 2 but for the cluster with an orbital eccentricity of 0.25. The four snapshots show the cluster and the corresponding streaklines in four different orbital phases (see also Tab. 1).  $\Delta x$  was chosen to be 60 pc just like in Fig. 2. The epicyclic movement gets distorted due to the eccentric cluster orbit. At apogalacticon (upper left panel) the epicycles are squeezed together, whereas at perigalacticon (upper right panel) the streaklines are stretched. In between these two orbital phases the shape of the streaklines differs if the cluster and its tails are being accelerated (lower left panel) or decelerated (lower right panel). Moreover, we get epicyclic movement also for the case when the test particles are released from the cluster with the same orbital velocity as the cluster (red solid lines).

cluster mass has so far been neglected but will, of course, influence the trajectories of escaping stars. The cluster can attract stars and even re-capture them if they happen to lie beyond the tidal radius (given by Eq. 2) at some later orbital phase. Read et al. (2006), for example, demonstrated that stars orbiting the cluster on prograde orbits with respect to the cluster motion about the galactic centre can escape the cluster potential more easily than stars on retrograde orbits. We therefore have to consider from which radius we release the test particles to produce the streaklines.

If we chose to release the test particles from the apogalactic tidal radius, which is the largest tidal radius throughout the orbit since the cluster has the lowest angular velocity at this point (see Tab. 1), then we may expect that virtually all test particles will escape the gravitational attraction of the cluster mass. This, however, might not be the most realistic approach. If we, on the other hand, chose to release the test particles always from the actual tidal radius,  $x_L(t)$  (Eq. 2), at the given time,  $t$ , then many test particles may be re-captured. This will especially be a problem

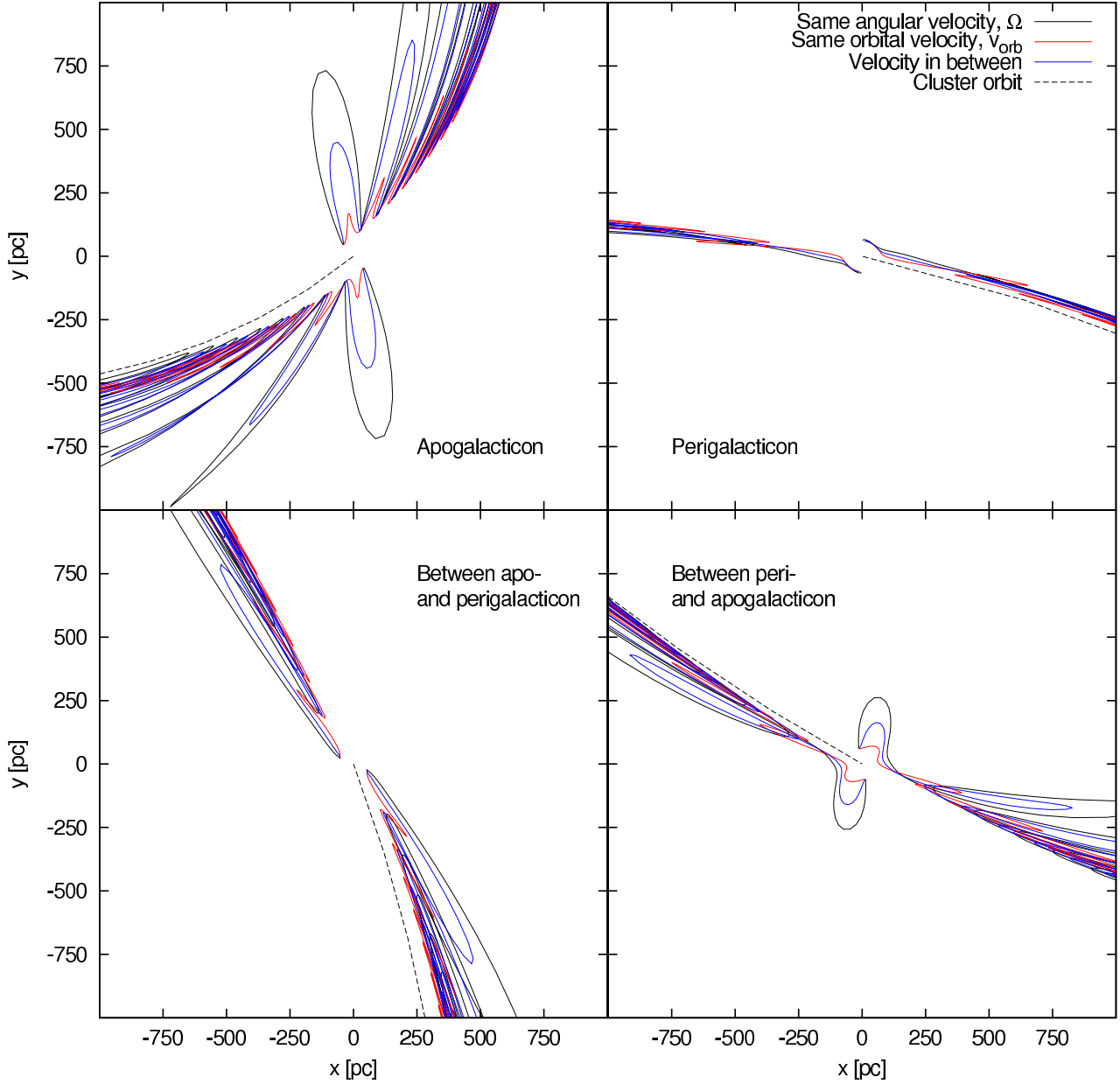


**Figure 4.** The same as Fig. 3 but for an orbital eccentricity of 0.5. Again, the four snapshots show four different orbital phases (see also Tab. 1). In this case  $\Delta x$  was also chosen to be 60 pc just like in Fig. 2. We see that the distortion effects get stronger with increasing eccentricity. The compression at apogalacticon is stronger than in Fig. 3, and so is the stretching at perigalacticon. Moreover, we can observe the effect of differential acceleration along the cluster-tail system. For example in the lower right panel the leading tail (to the right) is broader than the trailing tail.

for the test particles released near perigalacticon since the tidal radius is smallest here and, in addition, changes rapidly in this orbital phase as the angular velocity is largest at this point.

As we will demonstrate later, for this reason it is necessary to introduce a minimum radius from which test particles can be released such that no test particles gets re-captured. This radius we call the “edge” radius,  $x_{edge}$ , and it serves as a lower limit to the actual radius from which test particles will be released, i.e.

$$\Delta x(t) = \max(x_L(t), x_{edge}). \quad (15)$$

We determine the value of this edge radius by incrementally increasing the lower limit from the value of the perigalactic tidal radius until no test particle is re-captured.

In the following we will show that, for circular cluster orbits, this edge radius coincides with the constant tidal radius, since any particle released from rest from a smaller cluster radius will not be able to escape from the cluster potential (for the given escape conditions (i)-(iii)). For eccentric orbits this value is smaller than the apogalactic tidal radius but significantly larger than the perigalactic tidal radius. Its value decreases with increasing eccentricity for fixed apocentric distance.

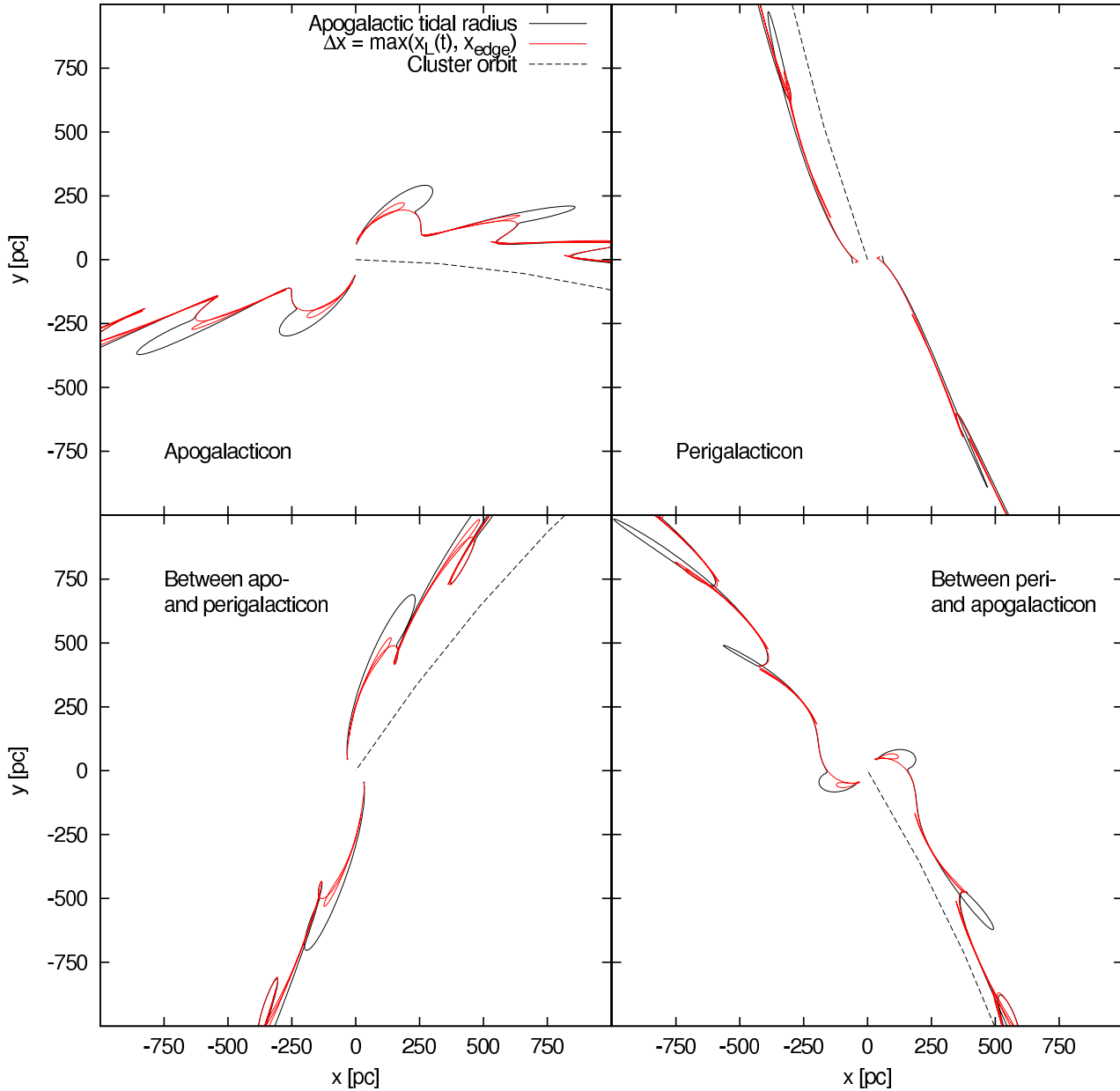


**Figure 5.** The same as Fig. 3 but here the cluster mass is taken into account. For the black solid lines the test particles were released from the cluster’s apogalactic tidal radius. The cluster mass was chosen such that the apogalactic tidal radius is 60 pc. The lines are similar to the lines for which the cluster mass was neglected (black solid lines in Fig. 3). When the test particles are released from the actual tidal radius of the cluster (red solid lines), the influence of the cluster mass gets more pronounced, as can be seen in the additional loops and bends. To produce these streaklines we had to introduce a minimum radius from which particles were released,  $x_{\text{edge}}$ , since else some test particles would have been re-captured by the cluster at a later orbital phase. This “edge” radius is 49.0 pc, whereas its perigalactic tidal radius is 37.5 pc.

## 2.4 Circular orbit

In the left panel of Fig. 2 the resulting streaklines for the circular cluster orbit are shown. The dashed line gives the orbit of the cluster. Along this orbit test particles have been released in constant time intervals with a positive or negative spatial offset,  $\Delta x$ , from the cluster centre along the galactocentric radius vector and with one of the three velocity offsets,  $v_t$ , given above. We chose  $\Delta x$  to be 60 pc, which is a somewhat arbitrary choice. The cluster and the test particles have each been independently integrated to the point

in time of the snapshot. Hence, there is no gravitational influence of the cluster on the test particles.

From the left panel of Fig. 2 it can be seen that the analytical results of Küpper, MacLeod & Heggie (2008a) and Just et al. (2009) are nicely reproduced when the test particles are released with the same angular velocity as the cluster (black solid line). Moreover, if the orbital velocity of the test particles at the larger (smaller) galactocentric radius is lower (higher) than in the case of equal angular velocity, the length of the epicycle is shorter (blue solid line).

In the case when the test particles have the same orbital



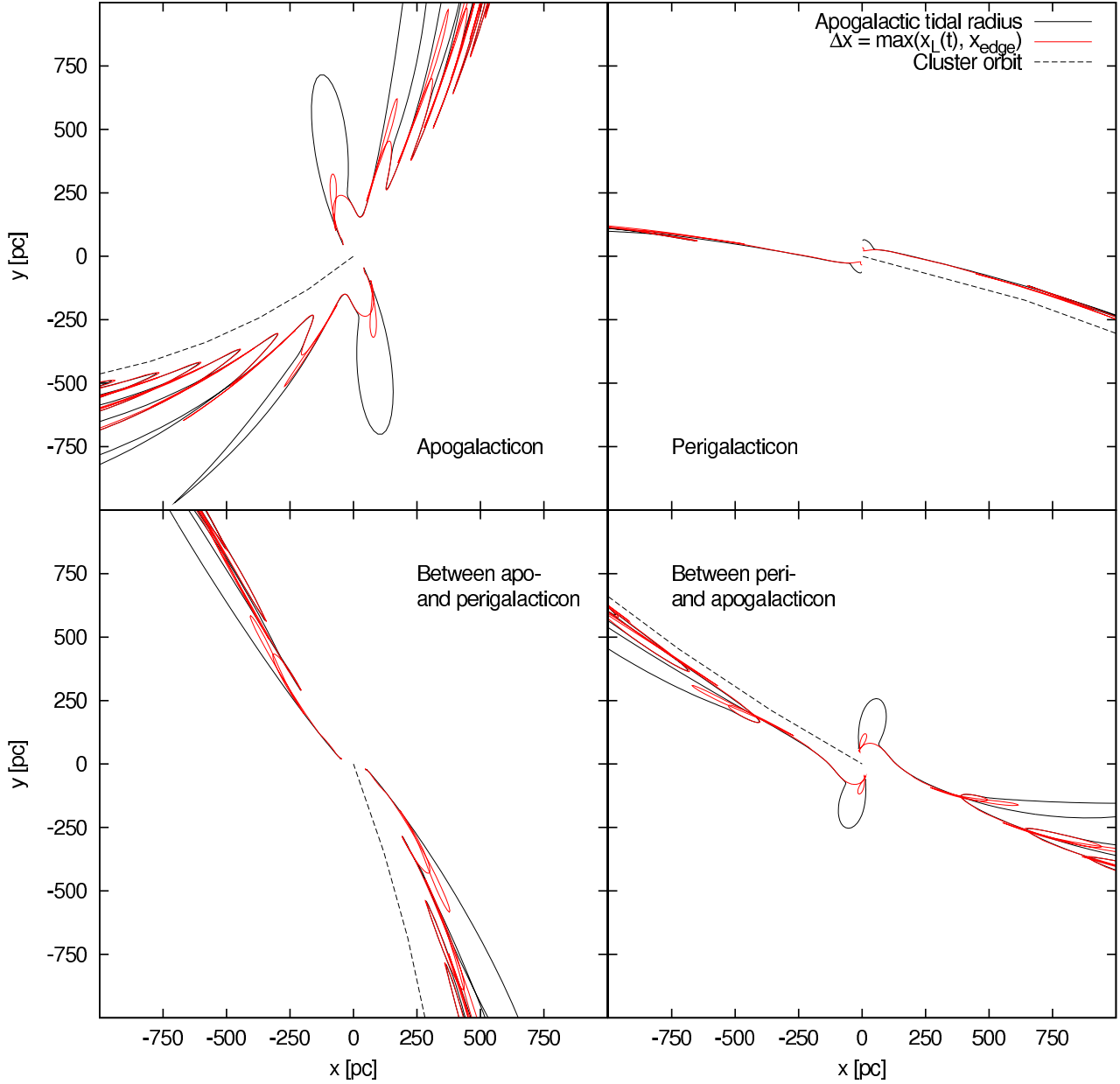


**Figure 6.** The same as Fig. 5 but for the cluster on an orbit with eccentricity of 0.5. Again, the cluster mass was chosen such that the apogalactic tidal radius is 60 pc. The streaklines for which the test particles were released from the apogalactic tidal radius (black solid lines) are again similar to the streaklines for which the cluster mass was neglected (black solid lines in Fig. 4). When the test particles are released from the actual tidal radius the streaklines get much more complex (red solid lines). For these streaklines we had to assume an edge radius 32 pc, whereas the perigalactic tidal radius is 21.2 pc.

velocity as the cluster then the epicycles should, in principle, be half as short as in the case of sharing the cluster's angular velocity, since

$$y_C = 3\pi \left( \Delta x + \frac{-\Omega \Delta x}{2\Omega} \right) = 3\pi \frac{\Delta x}{2}. \quad (16)$$

Instead, we see that the test particles follow a circular orbit (red solid line). From Eq. 8 we see that, in the case when  $v_t = -\Omega \Delta x$ , the radial extrema in the epicycles are at

$$x_m = 2\Delta x + \frac{v_t}{\Omega} \pm \left| \Delta x + \frac{v_t}{\Omega} \right| = \Delta x \pm 0. \quad (17)$$

Hence, the radial amplitude is zero, and the test particles

are moving on a circular orbit about the galactic centre with a radial offset to the cluster of size  $\Delta x$ .

The theoretical framework (Eq. 3–8) is in perfect agreement with our streaklines. Now we include the gravitational attraction of the cluster in our computations. The mass of the cluster in this computation is chosen such that the tidal radius,  $x_L$  (Eq. 2), coincides with the starting point of the test particles,  $\Delta x$ , i.e. 60 pc in our example.

As we can see in the right panel of Fig. 2, the cluster mass increases the length of the epicycles,  $y_C$ , by about 25%. Moreover, the sharp cusp at  $y_C$  is replaced by a smooth minimum, and the radial distance of the test particles from the

cluster orbit,  $\Delta x$ , is larger on average. The radial amplitude appears to be damped by a factor of about 0.6 when the cluster mass is taken into account.

All these effects can be explained when looking at the shape of the effective potential of cluster and galaxy near the tidal radius (see e.g. figure 2 of Just et al. 2009). Beyond the tidal radius the effective potential is repulsive such that the test particles get accelerated away from the cluster. Just et al. (2009) found that, due to Jacobi-energy conservation (see e.g. Heggie & Hut 2003), a test particle starting at  $\Delta x = x_L$  with  $v_t = 0$  will be at  $\Delta x = \sqrt{3}x_L$  if it ever comes to rest again in the future. In fact, the test particles in the minimum of our example are less than 10% off this value as they still have a velocity of 0.5 km/s with respect to their initial conditions.

Note that, since the distance of the Lagrange points as well as the length of the epicycles scales with the mass of the cluster, the effect of the cluster mass on the trajectories will always be the same. Stars escaping from a larger radius than the tidal radius will, of course, be less influenced by the cluster mass. Their trajectories will look more like the ones for which we neglected the cluster mass.

## 2.5 Eccentric orbits

In Fig. 3 the streaklines of the cluster in an eccentric orbit with eccentricity 0.25 are shown for four different orbital phases. Here, again, the cluster mass was neglected. Also, we chose  $\Delta x$  to be 60 pc like in the previous example. We see that the streaklines are distorted in comparison to the circular orbit case (Fig. 2). Moreover, the distortion depends on the orbital phase of the cluster. At apogalacticon the streaklines appear to be similar to the circular orbit case but squeezed together. The length of the epicycles is much shorter than in the circular orbit case and epicyclic loops further away from the cluster are tilted towards the cluster orbit.

Between apo- and perigalacticon, when the cluster and the test particles are accelerated towards the galactic centre, the tilt of the epicyclic loops gets stronger, whereas the length of the epicycles increases. At perigalacticon the epicyclic loops are almost completely aligned with the cluster orbit. The length of the epicycles is largest in this orbital phase. Between peri- and apogalacticon, when the cluster and the test particles are decelerated, the tilt gets weaker, the epicycles shorter and the loop structure gets more pronounced.

Also apparent from Fig. 3 is the thickness of the tidal tails. Assuming that most stars follow such an epicyclic motion, we can expect the tidal tails to be thickest at apogalacticon and thinnest at perigalacticon. Moreover, we see that we get epicyclic motion even when the escaping stars have the same orbital velocity as the cluster. This is due to the stars and the cluster being on slightly different eccentric orbits about the galactic centre. The same is shown in Fig. 4 for the cluster with an orbital eccentricity of 0.5. All effects described above get more pronounced. Furthermore, with increasing orbital eccentricity it gets more difficult to separate the individual streaklines as the epicyclic loops overlap multiply.

In these illustrations the offset radius,  $\Delta x$ , from which the test particles have been released were the same for all

snapshots. When we take the cluster mass into account in our computations then we can fix  $\Delta x$  to the apogalactic tidal radius in order to be able to better compare the resulting streaklines to Fig. 3 & 4. Therefore we chose the cluster mass such that the apogalactic tidal radius is 60 pc. The streaklines are shown in Fig. 5 (black solid lines) for the cluster on an orbit with eccentricity of 0.25. As we can see, the streaklines look quite similar to the lines for which the cluster mass was neglected (black solid lines in Fig. 3). Only some minor bends in the lines tell us that there is some influence of the cluster on the test particles.

This changes when we release particles from the actual tidal radius (Eq. 2). The influence of the cluster mass on the test particles gets much more obvious, as the lines show additional loops and bends (red solid lines). To produce the streaklines in Fig. 5 we had to introduce a minimum radius from which we release particles, the “edge” radius,  $x_{edge}$ , mentioned above (Sec. 2.3, Eq. 15). For the orbit with an eccentricity of 0.25 this edge radius was found to be 49.0 pc (about 80% of the apogalactic tidal radius), whereas its perigalactic tidal radius is 37.5 pc.

Both sets of streaklines are shown in Fig. 6 for the cluster on an orbit with an eccentricity of 0.5. Here again we adjusted the cluster mass such that the apogalactic tidal radius is 60 pc. The effects described above get more pronounced. For the black solid lines the test particles were released from the apogalactic tidal radius, and for the red solid lines they were released from the actual tidal radius. The edge radius, which we had to introduce here as well, is 32.0 pc (about 50% of the apogalactic tidal radius), whereas the perigalactic tidal radius is 21.2 pc.

## 3 COMPARISON WITH *N*-BODY DATA

The three *N*-body computations which we use here for comparison with streaklines are taken from Küpper et al. (2010a). The models were set-up using the publicly available code MCLUSTER<sup>1</sup> (Küpper et al. 2011b). They initially consist of 65536 stars drawn from the canonical initial mass function (Kroupa 2001, eq. 2) with masses between  $0.1 M_\odot$  and  $1.2 M_\odot$ , resulting in a cluster mass of about  $20000 M_\odot$ . The cluster stars follow a Plummer density profile with a half-mass radius of 8 pc.

The clusters are initially located at their apocentre of 8.5 kpc within an Milky Way-like potential (Allen & Santillan 1991; see Sec. 2.2). We chose three orbital eccentricities for the clusters of  $\epsilon = \{0.00, 0.25, 0.50\}$ , which start with an orbital velocity of  $v_{orb} = \{220, 165, 110\}$  km s<sup>-1</sup>. From Eq. 1 we can infer that the tidal radius of these clusters is of the order of 40 pc. Hence, with a ratio of half-mass radius to tidal radius of about 0.2 the models belong to the group of extended, tidally filling clusters as categorised by Baumgardt et al. (2010).

The computations were performed with NBODY4 (Aarseth 2003) on the GRAPE special-purpose computers (Fukushige, Makino & Kawai 2005) at AIfA Bonn for 4 Gyr. Here we use snapshots in the middle of these computations

<sup>1</sup> [www.astro.uni-bonn.de/~akuepper/mcluster/mcluster.html](http://www.astro.uni-bonn.de/~akuepper/mcluster/mcluster.html)  
or [www.astro.uni-bonn.de/~webaiub/german/downloads.php](http://www.astro.uni-bonn.de/~webaiub/german/downloads.php)

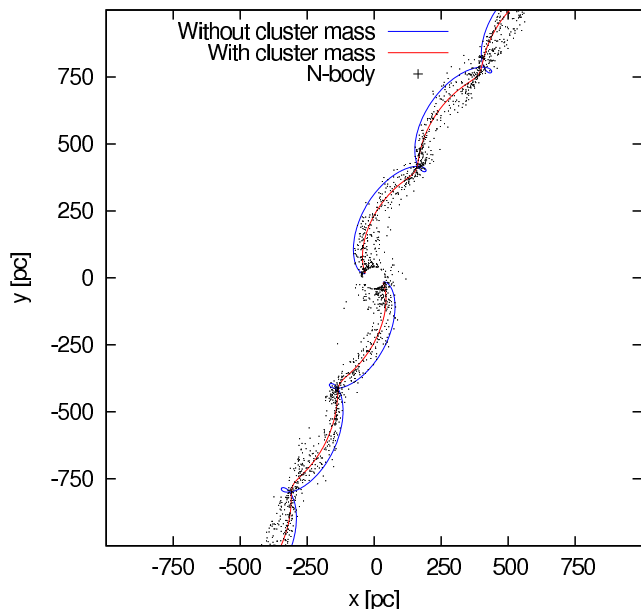


**Figure 7.** Comparison of streaklines to results from  $N$ -body computations of a cluster on a circular orbit. The cluster was integrated for 2 Gyr and has lost about  $3600 M_{\odot}$  of stars which are mainly in the tidal tails now (black dots; stars within a cluster radius of 40 pc were omitted for clarity). The blue solid lines show the streaklines for which the cluster mass was neglected. To match the length of the epicyclic overdensities, the test particles were released with a tangential velocity of  $v_t = 0.55 \text{ km s}^{-1}$  from the cluster's tidal radius, i.e.  $\Delta x = x_L = 37 \text{ pc}$ . For the red solid lines the cluster mass was taken into account. The test particles were released from the cluster's tidal radius with zero velocity. As we can see, the shape of the tails is much better reproduced by the streaklines which take the cluster mass into account. The scatter of stars about this streakline may well originate from the scatter in escape conditions.

at different orbital phases as shown in Fig. 1 and summarised in Tab. 1.

### 3.1 Circular orbit

The first snapshot (Fig. 7) is from the cluster on a circular orbit after 2 Gyr of dynamical evolution. The star cluster is shown in projection onto the orbital plane similar to Fig. 2. It has lost about  $3600 M_{\odot}$ , of which most stars escaped into the tidal tails (black dots in Fig. 7; stars within a cluster radius of 40 pc are not shown for clarity). The predicted over- and underdensity pattern is clearly visible in both the leading and the trailing tail. Moreover, we see that the tidal tails have a rolling shape, resulting from the epicyclic motion of the tail stars.

The tidal radius,  $x_L$  (Eq. 2), of the cluster at this moment is 37 pc, so from Eq. 4 we expect the length of the epicycles,  $y_C$ , to be about 350 pc when the stars escape with zero tangential velocity,  $v_t$ . We find, however, that they are closer to 400-500 pc. In Küpper et al. (2010a) we argued that this is due to the cluster stars escaping with small excess velocities of about  $0.27\text{-}0.55 \text{ km s}^{-1}$  in the direction of the tails. This is a reasonable assumption, since such excess velocities have been measured for evaporating stars in  $N$ -body simulations. Küpper, Kroupa & Baumgardt (2008b) found

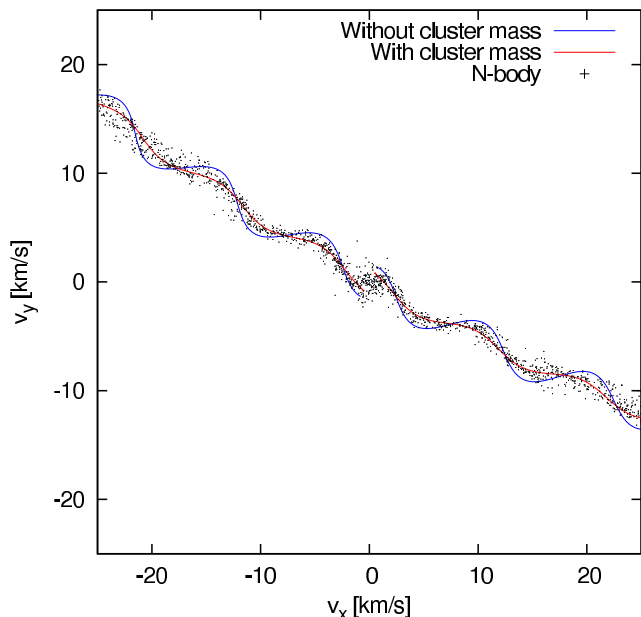


**Figure 8.** The same as Fig. 7 but in velocity space (velocities are given with respect to the cluster velocity). Black dots show more or less the same stars from the  $N$ -body simulation as shown in Fig. 7. Here stars within a cluster radius of 40 pc were again omitted for clarity. As in Fig. 7 the blue solid lines show the streaklines for which the cluster mass was neglected, whereas for the red solid lines the cluster mass was taken into account. Also in velocity space the shape of the tails is much better reproduced by the streaklines which take the cluster mass into account.

the velocities of evaporating stars to be of a log-normal distribution with a peak at roughly the mean stellar velocity within the cluster. Also, it is clear from Fig. 2 that, in our simple model, the distance between overdensities depends on the velocity with which escapers are released. Nevertheless the streaklines shown in Fig. 7 were generated from a single value of the initial velocity, which we have found to produce a satisfactory fit to the structure of the tidal tails.

The streaklines of these assumed escape conditions are shown in blue in Fig. 7. As we can see, the epicyclic pattern is well reproduced, that is the epicycles have the correct length. Nevertheless, these streaklines do not seem to perfectly describe the motion of escaping stars. It seems like most escapers rather follow trajectories which are less curved and which are closer to the cluster orbit on average. However, we neglected the cluster mass for these streaklines.

For the red solid lines in Fig. 7 the cluster mass was taken into account. The test particles were released with zero velocity from the tidal radius in this case. The streaklines seem to perfectly match the mean path of the escaping stars, therefore they reflect the dominant mode of escape. The scatter about this mean path may well be due to the scatter in escape conditions mentioned above.

In Fig. 8 the comparison between the  $N$ -body data and our simple streakline model is shown as in Fig. 7 but now in velocity space. The epicyclic motion of tail stars can also be seen as a periodic velocity variation. Like in Fig. 7 we can see that the  $N$ -body data is reproduced better by the streaklines for which the cluster mass is taken into account. Our simple model therefore seems to represent the average

escape conditions. As can be seen in Figs. 7 & 8, the deviations from these average escape conditions are relatively small.

### 3.2 Eccentric orbits

In Fig. 9 the four consecutive snapshots of the cluster on an orbit with an eccentricity of 0.25 are shown. The cluster has lost about  $5000 M_{\odot}$  of stars which are mainly in the tidal tails (black dots). Here, again, the epicyclic movement of the tail stars is visible. The tails show periodic overdensities with a distance from the cluster which varies with the orbital period (as observed by Küpper et al. 2010a). At apogalacticon the overdensities are close to the cluster, whereas they are furthest away at perigalacticon.

Also the shape of the tails depends on the orbital phase. At apogalacticon they appear similar to the circular orbit case with the rolling shape. However, the tails are denser and broader as they are being compressed due to differential acceleration across the tails. At perigalacticon the tails are thinnest and they appear almost like straight lines. The two snapshots in between appear quite different even though the cluster is in a similar orbital phase, only being accelerated in the one snapshot and decelerated in the other. The distance of the overdensities is comparable, whereas the shape of the tails is very distinct. In between peri- and apogalacticon the tails show prominent streaks like have often been observed in numerical simulations before (Dehnen et al. 2004; Capuzzo Dolcetta, Di Matteo & Miocchi 2005; Montuori et al. 2007), but which have not yet been assigned to epicyclic motion of tail stars. These features may also be the true nature of the multiple tidal tails observed for Galactic satellites like NGC 288, Willman 1 and NGC 2298 (Leon, Meylan & Combes 2000; Willman et al. 2006; Balbinot et al. 2011).

Also shown are streaklines for which the test particles have been released from the actual tidal radius (Eq. 2). However, since the tidal radius at perigalacticon is very small (24.8 pc) and the passage through perigalacticon is quite fast, there are many test particles which get re-captured from the cluster as it moves to apogalacticon. Therefore, we had to introduce a minimum radius,  $x_{edge}$ , from which test particles are released (see Sec. 2.3, Eq. 15). This “edge” radius was found to be 32.5 pc by incrementing its size from zero until no test particles was re-captured. Its size is about 80% of the cluster’s apogalactic tidal radius (39.5 pc). Remarkably, with this minimal choice of edge radius the streaklines reproduce the  $N$ -body data very well, even though their shape is very sensitive to this value.

In Fig. 10 the four consecutive snapshots of the cluster on an orbit with  $\epsilon = 0.5$  are shown. This cluster has already lost  $10500 M_{\odot}$  of stars which are now mainly in the tidal tails (black dots). The orbital compression of the tails gets stronger at apogalacticon. The overdensities are very close to each other and the tails are very broad. Moreover, they show prominent streaky features. At perigalacticon the tails become even thinner than in the  $\epsilon = 0.25$  case. From the snapshot between peri- and apogalacticon we can see that the cluster-tail system is experiencing severe differential acceleration, such that the leading tail (to the right) is already being broadened, whereas the trailing tail is still quite thin.

The red solid lines in Fig. 10 have been produced by re-

leasing test particles from the actual tidal radius and assuming a minimum tidal radius (edge radius) of 18.0 pc (Eq. 15). The perigalactic tidal radius of this cluster is 12.9 pc and the apogalactic tidal radius is 36.4 pc. Hence, the edge radius is about 50% of the apogalactic tidal radius. Again, as for the cluster with an orbital eccentricity of 0.25, this choice of escape conditions reproduces the  $N$ -body data remarkably well.

Finally, from Fig. 9 & 10 it is obvious that all substructure within the tidal tails can be ascribed to epicyclic motion of tail stars. This rules out tidal shocks as origin of substructure in these systems. Moreover, it demonstrates how complex the motion of stars within tidal tails of star clusters like Pal 5 can be, and thus how unlikely the formation of overdensities in such tidal tails through Jeans instabilities is (Quillen & Comporetta 2010; Schneider & Moore 2011).

## 4 SUMMARY AND CONCLUSIONS

We have investigated the motion of stars escaping from star clusters using streaklines (for details on streaklines see Sec. 2.3), focussing on three star cluster models with orbital eccentricities of 0.0, 0.25 and 0.5 (further description of the models in Sec. 2.2). We demonstrated how escaping stars move on epicycles within tidal tails (Sec. 2.4 & 2.5), and that this epicyclic motion is the only origin of the substructure observed in  $N$ -body computations of dissolving star clusters (Sec. 3).

In Küpper, MacLeod & Hoggie (2008a) it was shown analytically and numerically for circular cluster orbits, how the length of the epicycles changes with the size of the radial offset,  $\Delta x$ , escaping stars have with respect to the cluster orbit at the moment of escape. Here we visualised, with the help of streaklines, how the shape of the epicycles changes when we vary the tangential velocity,  $v_t$ , of the escaping stars. In fact, the shape of the epicycles and thus the tidal tails is very sensitive to this velocity. Furthermore, we demonstrated how this motion gets distorted when the cluster orbit is eccentric, and what (important) influence the cluster mass has.

When a cluster on an eccentric orbit is close to apogalacticon then the epicyclic motion of stars within its tails may lead to streaks appearing like multiple tails. Such features have been observed in numerical simulations before (Dehnen et al. 2004; Capuzzo Dolcetta, Di Matteo & Miocchi 2005; Montuori et al. 2007), but have not yet been interpreted as result of epicyclic motion. The streaks may also be the true nature of the multiple tidal tails observed for Galactic satellites like NGC 288, Willman 1 and NGC 2298 (Leon, Meylan & Combes 2000; Willman et al. 2006; Balbinot et al. 2011).

Finally, we compared sets of streaklines to results from three  $N$ -body models following the same orbits as stated above. We found that the tidal tails of these computations can be accurately reproduced by a quite simple model, that is when we assume that the stars evaporate from the actual tidal radius,  $x_L(t)$ , the star cluster has at the moment when the star escapes. When the velocity of the escapers is chosen such that they have the same angular velocity as the cluster,

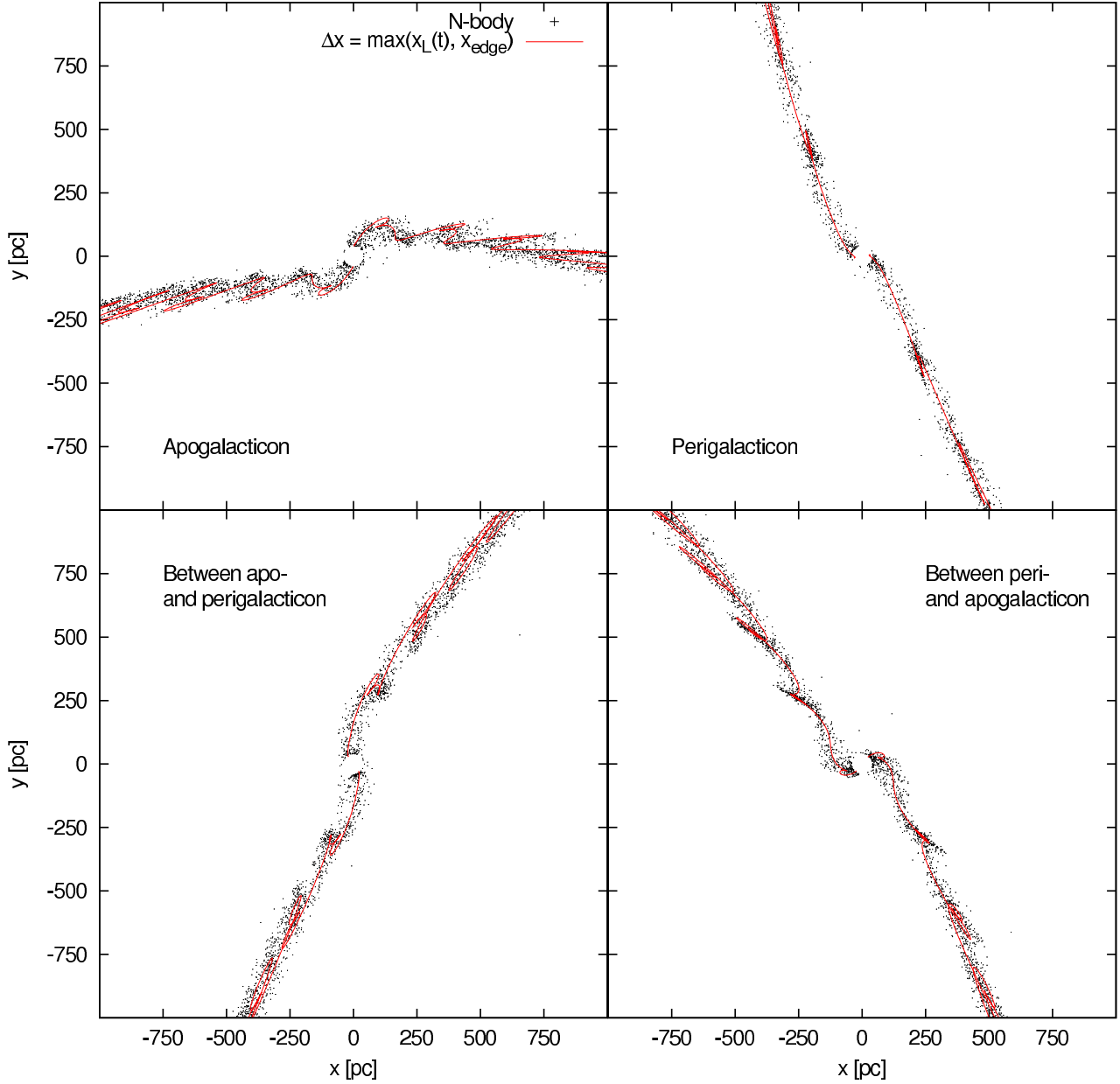


**Figure 9.** The same as Fig. 7 but for the cluster with an orbital eccentricity of 0.25. This cluster has lost already  $5000 M_{\odot}$  of stars (black dots; stars within a cluster radius of 40 pc were omitted for clarity). As in Fig. 3 & 5, the four snapshots show the cluster in four different orbital phases. The shape and density of the tidal tails changes significantly during one orbit. At apogalacticon they look similar to the circular orbit case but squeezed together. At perigalacticon the tails are stretched and the overdensities are much further away from the cluster than at apogalacticon. The orbital phases in between look quite distinct: between peri- and apogalacticon the tails show a streaky structure which has often been observed in numerical simulations. Also shown are streaklines for which the test particles have been released from the actual tidal radius (Eq. 15) with zero velocity (red solid lines). The edge radius which was used here is 32.5 pc, in comparison to the 24.8 pc perigalactic tidal radius and the 39.5 pc apogalactic tidal radius. This set-up can reproduce all four snapshots without further ado, and especially reproduces the streaky features between peri- and apogalacticon. Such features have often been interpreted as results of tidal shocks in the past.

the shape of the tidal tails is reproduced best. This is what we find to be the dominant mode of escape.

However, we have to assume that there is a lower limit,  $x_{edge}$ , to the tidal radius. That is, stars escape from  $\Delta x(t) = \max(x_L(t), x_{edge})$ . This “edge” radius was found to be identical to the tidal radius of the cluster, if it moves on a circular orbit, but was found to decrease with increasing orbital eccentricity at fixed apocentric distance. For all

orbits, the edge radius turned out to be significantly larger than the corresponding perigalactic tidal radius. It can be interpreted as the minimum radius from which a star can escape from the cluster during one cluster orbit without being re-captured by the cluster in a later orbital phase.

These findings have only been established, however, for systems where the escape of stars is dominated by collisional heating, on galactic orbits with eccentricities up to 0.5. For

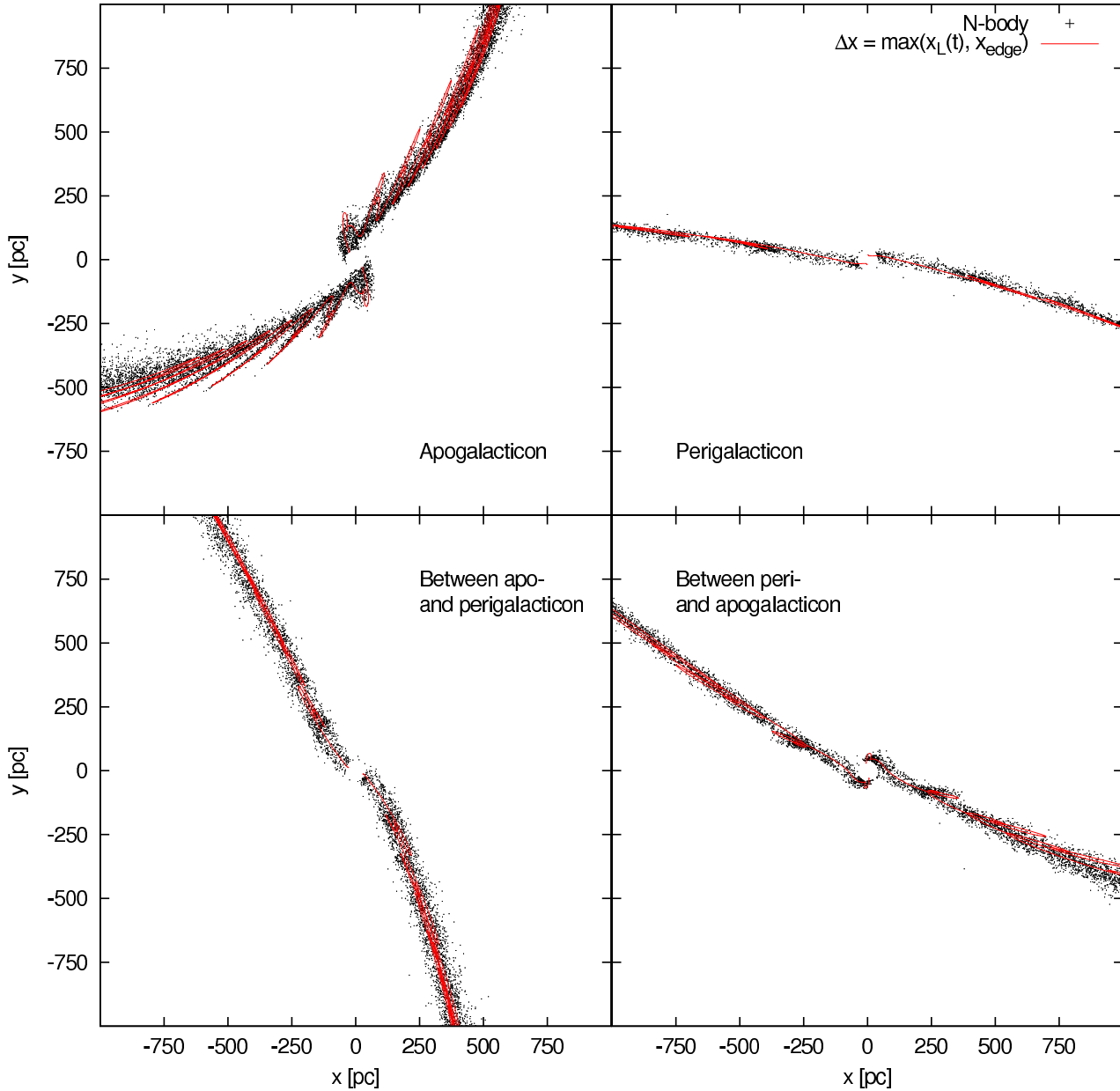


**Figure 10.** The same as Fig. 7 & 9 but for an orbital eccentricity of 0.5. Due to the high eccentricity, this cluster has already lost  $10500 M_{\odot}$  of stars (black dots; stars within a cluster radius of 40 pc were omitted for clarity). Here, like in Fig. 4, the four snapshots show four different orbital phases. We see that the compression and stretching of the tails gets more pronounced with increasing orbital eccentricity. Furthermore, at apogalacticon the compressed epicyclic loops appear like streaky features. These structures can be well reproduced by streaklines, when we release the test particles from the actual tidal radius (red solid lines). The edge radius we used here is 18.0 pc, in comparison to the 12.9 pc perigalactic tidal radius and the 36.4 pc apogalactic tidal radius.

much larger eccentricities, or any other system where mass loss may be dominated by tidal heating, modelling the structure of tidal tails may require refinement, as suggested by the collisionless modelling in Peñarrubia et al. (2009). Even in the case of a cluster on a circular galactic orbit, the notion of a single escape radius is over-simplistic (Read et al. 2006), but even these authors find that, in the long run, the “tidal radii” of stars on prograde, circular and retrograde orbits tend to a single value.

Küpper et al. (2010b) investigated in detail the same three *N*-body models that we discuss in the present pa-

per. They found that all three models show a radial density profile which barely changes with time. By fitting King profiles (King 1962) and a new, so-called, KKBH profile, they showed that the fitted tidal radius does not change with the orbital period, even though Eq. 2 would suggest that the tidal radius should be large at apogalacticon and small at perigalacticon. For this reason they suggested to rather name such a fitted tidal radius the “edge” radius. Furthermore, they found that the fitted edge radius of the model on a circular orbit is close to its true tidal radius of 37 pc, whereas the model with an orbital eccentricity of

0.25 showed an edge radius of about 30 pc, and the one with  $\epsilon = 0.5$  had a constant edge radius of about 20 pc. These values lie remarkably close to the values we found by adjusting streaklines to the tidal tails of these  $N$ -body models.

These results suggest that the edge radius is fundamentally connected to the orbit of a star cluster and its mass. Stars preferentially evaporate from the actual tidal radius of the cluster whose lower limit is given by the edge radius. That is, stars within the edge radius cannot escape, whereas stars outside the edge radius get “eaten away” by the tide. This edge radius can be recovered by fitting a King or a KKBH profile to the radial density profile. It must be mentioned, though, that these findings will most likely only hold for extended, tidally filling clusters (see Baumgardt et al. 2010) with a ratio of half-mass radius to tidal radius larger than approximately 0.1, since more concentrated clusters may not have properly adapted to the mean tidal field yet.

Furthermore, applying our results to dwarf spheroidal galaxies may be complicated by the fact that in such systems the crossing time of stars orbiting at large radii may easily exceed the orbital time of the dwarf galaxy about its host. Instead, Peñarrubia et al. (2009) find that in dwarf galaxies which experienced a recent tidal shock an edge develops which moves radially outward with time. Such a dwarf galaxy will lose most of its mass due to tidal stripping rather than through dynamical evaporation. The scatter in escape conditions of escaping stars would be much higher in this case so that our simple model would not work for the majority of escapers. Thus, no pronounced epicyclic signature would be expected for the tidal tails of such objects.

Originally, King (1962) suggested that the observed cut-off radius, i.e. edge radius, of a star cluster on an eccentric cluster orbit is related to its respective perigalactic tidal radius

$$x_t^{peri} = \left( \frac{GM}{(2 + \epsilon)\Omega_{peri}^2} \right)^{1/3}, \quad (18)$$

where  $\Omega_{peri}$  is the cluster’s angular velocity at perigalacticon. Hence, the cut-off radius should be even significantly smaller than the perigalactic tidal radius for high eccentricities. Similar results have been found by Read et al. (2006) and Kennedy (2011), both predicting the cut-off radius to be of the order of the perigalactic tidal radius. In contrast to this, we found the edge radius of clusters on eccentric orbits to be significantly larger than the perigalactic radius. The reason for this difference is that stars that become unbound at perigalacticon at smaller radii get re-captured by the cluster at a later orbital phase.

Finally we conclude that, if sufficient information on a specific globular cluster of the Milky Way is available, this knowledge on the formation of tidal debris can be used to predict the shape of its tidal tails and the location of its epicyclic overdensities. In a future investigation we are going to demonstrate this with the globular cluster 47 Tucanae (Lane, Küpper & Heggie, in prep.). Moreover, we would like to point out that epicyclic motion of stars within tidal tails of star clusters leads to over- and underdensities independent from the cluster orbit about the host galaxy. Therefore substructure in tidal tails is not necessarily due to substructure in the galactic potential like spiral arms, giant molecular clouds or dark-matter subhaloes (e.g. Ibata et al. 2002; Carlberg 2009).

## ACKNOWLEDGMENTS

The authors are grateful to Sverre Aarseth for making his NBODY codes accessible to the public. Moreover they would like to thank Jorge Peñarrubia for useful comments. AHWK kindly acknowledges the support of an ESO Studentship and through the German Research Foundation (DFG) project KR 1635/28-1. RRL acknowledges support from the Chilean Center for Astrophysics, FONDAPE Nr. 15010003, the BASAL Centro de Astrofísica y Tecnologías Afines (CATA) PFB-06/2007 and the GEMINI-CONICYT Fund, allocated to project No. 32090010.

## REFERENCES

- Aarseth S. J., 2003, *Gravitational N-Body Simulations*, Cambridge, UK, Cambridge University Press
- Allen C., Santillan A., 1991, *RMxAA*, 22, 255
- Balbinot E., Santiago B. X., da Costa L. N., Makler M., Maia M. A. G., 2011, *MNRAS*, 416, 393
- Baumgardt H., Makino J., 2003, *MNRAS*, 340, 227
- Baumgardt H., Parmentier G., Gieles M., Vesperini E., 2010, *MNRAS*, 401, 1832
- Belokurov V., et al., 2006, *ApJ*, 642, L137
- Binney J., 2008, *MNRAS*, 386, L47
- Capuzzo Dolcetta R., Di Matteo P., Miocchi P., 2005, *AJ*, 129, 1906
- Carlberg R. G., 2009, *ApJ*, 705, L223
- Chandrasekhar S., 1942, *Principles of Stellar Dynamics*, Chicago, Ill., The University of Chicago Press
- Dehnen W., Odenkirchen M., Grebel E. K., Rix H.-W., 2004, *AJ*, 127, 2753
- Drukier G. A., Slavin S. D., Cohn H. N., Lugger P. M., Berrington R. C., Murphy B. W., Seitzer P. O., 1998, *AJ*, 115, 708
- Eyre A., Binney J., 2009a, *MNRAS*, 399, L160
- Eyre A., Binney J., 2009b, *MNRAS*, 400, 548
- Fellhauer M., et al., 2006, *ApJ*, 651, 167
- Fukushige T., Heggie D. C., 2000, *MNRAS*, 318, 753
- Fukushige T., Makino J., Kawai A., 2005, *PASJ*, 57, 1009
- Gnedin O. Y., Ostriker J. P., 1997, *ApJ*, 474, 223
- Gnedin O. Y., Lee H. M., Ostriker J. P., 1999, *ApJ*, 522, 935
- Grillmair C. J., Johnson R., 2006, *ApJ*, 639, L17
- Grillmair C. J., Dionatos O., 2006a, *ApJ*, 641, L37
- Grillmair C. J., Dionatos O., 2006b, *ApJ*, 643, L17
- Grillmair C. J., 2006, *ApJ*, 651, L29
- Heggie D., Hut P., 2003, *The Gravitational Million-Body Problem*, Cambridge, UK, Cambridge University Press
- Ibata R. A., Lewis G. F., Irwin M. J., Quinn T., 2002, *MNRAS*, 332, 915
- Johnston K. V., Zhao H., Spergel D. N., Hernquist L., 1999, *ApJ*, 512, L109
- Just A., Berczik P., Petrov M. I., Ernst A., 2009, *MNRAS*, 392, 969
- Kennedy G.F., 2011, *MNRAS* submitted (arXiv:1108.5241)
- King I., 1962, *AJ*, 67, 471
- Koposov S. E., Rix H.-W., Hogg D. W., 2010, *ApJ*, 712, 260
- Kroupa P., 2001, *MNRAS*, 322, 231
- Küpper A. H. W., MacLeod A., Heggie D. C., 2008a, *MNRAS*, 387, 1248

- Küpper A. H. W., Kroupa P., Baumgardt H., 2008b, MNRAS, 389, 889
- Küpper A. H. W., Kroupa P., Baumgardt H., Heggie D. C., 2010a, MNRAS, 401, 105
- Küpper A. H. W., Kroupa P., Baumgardt H., Heggie D. C., 2010b, MNRAS, 407, 2241
- Küpper A. H. W., Mieske S., Kroupa P., 2011a, MNRAS, 413, 863
- Küpper A. H. W., Maschberger T., Kroupa P., Baumgardt H., 2011b, MNRAS, 417, 2300
- Lane R. R., Kiss L. L., Lewis G. F., Ibata R. A., Siebert A., Bedding T. R., Székely P., 2009, MNRAS, 400, 917
- Lane R. R., Kiss L. L., Lewis G. F., Ibata R. A., Siebert A., Bedding T. R., Székely P., 2010a, MNRAS, 401, 2521
- Lane R. R., et al., 2010b, MNRAS, 406, 2732
- Law D. R., Johnston K. V., Majewski S. R., 2005, ApJ, 619, 807
- Leon S., Meylan G., Combes F., 2000, A&A, 359, 907
- Lin D. N. C., Lynden-Bell D., 1977, MNRAS, 181, 59
- Lynden-Bell D., Lynden-Bell R. M., 1995, MNRAS, 275, 429
- Miyamoto M., Nagai R., 1975, PASJ, 27, 533
- Montuori M., Capuzzo-Dolcetta R., Di Matteo P., Lepinette A., Miocchi P., 2007, ApJ, 659, 1212
- Odenkirchen M., et al., 2003, AJ, 126, 2385
- Odenkirchen M., Grebel E. K., Kayser A., Rix H.-W., Dehnen W., 2009, AJ, 137, 3378
- Peñarrubia J., et al., 2005, ApJ, 626, 128
- Peñarrubia J., Navarro J. F., McConnachie A. W., Martin N. F., 2009, ApJ, 698, 222
- Quillen A.C., Comparetta J., 2010, MNRAS submitted (arXiv:1002.4870)
- Read J. I., Wilkinson M. I., Evans N. W., Gilmore G., Kleya J. T., 2006, MNRAS, 366, 429
- Scarpa R., Marconi G., Gilmozzi R., Carraro G., 2007, A&A, 462, L9
- Scarpa R., Falomo R., 2010, A&A, 523, A43
- Scarpa R., Marconi G., Carraro G., Falomo R., Villanova S., 2011, A&A, 525, A148
- Schneider A., Moore B., 2011, MNRAS, 415, 1569
- Willman B., et al., 2006, arXiv:astro-ph/0603486
- Yanny B., et al., 2003, ApJ, 588, 824